EPJ Web of Conferences **23**, 00010 (2012)
DOI: 10.1051/epjconf/20122300010
© Owned by the authors, published by EDP Sciences, 2012

Resonant impurity scattering in the unconventional superconductors

Yunkyu Bang[1,a]

Department of Physics, Chonnam National University, Kwangju 500-757, Korea

Abstract. In this pedagogical review, I provide comparative studies of the impurity scattering effects on the two typical types of the unconventional superconductors: d-wave and ±s-wave superconductors. For the d-wave superconductor, the main effect of impurity scattering is the formation of the zero energy resonant state by the unitary scatters below T_c. Similarly, in the case of the ±s-wave superconductor, I show that impurity scattering of the unitary limit also forms a resonant bound state, however, not a zero energy but an off-centered bound state inside the superconducting (SC) gap, which modifies the density of states (DOS) of a fully opened gap to a V-shaped one mimicking the pure d-wave DOS. On the contrary, in the d-wave case, the zero energy bound state modifies the original V-shape DOS into a flat constant one near zero frequency. This contrasting behavior of the impurity effect can be useful to distinguish the gap symmetry of the newly discovered Fe-based superconductors. This contrasting behavior of two SC states with respect to the impurity scattering is demonstrated by numerical calculations of the density of states (DOS), NMR $1/T_1$ rate and Knight shift $K(T)$.

1 Introduction

The impurity scattering is an important and useful tool to study the superconducting (SC) gap symmetry because it distinguishes the phase of the gap. For example, it is well known that the conventional s-wave gap and the typical nodal gap superconductors(Ss) such as d-wave and p-wave can be easily distinguished by studying the impurity effects.

Especially the study of the impurity effects played a crucial role to understand the SC properties of the high-T_c cuprate superconductors (HTCSs) which is known to be a d-wave superconductor (S). It is well known that the impurity scattering in the d-wave S changes the power law dependencies of the various low energy SC properties compared to the pure d-wave state. For example, the temperature dependence of the penetration depth $\lambda(T)$ changes from the T-linear in the pure d-wave case to the T^2 behavior with impurities, which is well confirmed with experiments. Therefore it is very important to have a clear theoretical understanding of the impurity effects on the specific SC state to confidently identify the correct gap symmetry from the experimental data.

Recently, the Fe-based Ss have been discovered and attracted a great interest[1,2]. The issue of the gap symmetry of this new class of Sc is currently yet settled and hence the studies of impurity effects, both experimentally and theoretically, is important to clarify this issue. Among the candidate gap symmetries for the Fe-based S, the so-called ±s-wave state (or sign-changing s-wave state) is the most promising gap state[3–7]. As will be discussed in the main text, the ±s-wave state is, loosely speaking, a kind of hybrid of the d-wave gap and the s-wave gap, so that it is expected that the impurity effects on this SC state also show the interesting mixture behavior of the d-wave and the s-wave cases.

In this review, we introduce the T-matrix formalism for the impurity scattering in the SC state[8,9]. The T-matrix approximation has been successfully applied to the various unconventional superconductors such as heavy fermion [9] and high-temperature superconductors [10]. For example, it predicts a resonant bound state by unitary impurity scatterer inside the d-wave SC gap, which was crucial to explain the penetration depth of HTSC [10], $1/T_1$ experiments of Pu-115 superconductor[11], etc. We first start with the d-wave case and reproduce the known results for the pedagogical purpose. Then we generalize the formalism to the ±s-wave state of the minimal two band model[12] and provide comparative calculations of the impurity effects on several low energy SC properties to be compared to the d-wave case.

The interesting effect of impurities in the SC state occurs when the strong impurity scatterers form a impurity resonance inside the SC gap below T_c. The key principle of forming a resonance bound sate in the d-wave gap is that the sign-changing d-wave SC order parameter(OP) guarantees the absence of the renormalization of the anomalous selfenergy due to impurity scattering. In the case of the ±s-wave SC state, there are two s-wave OPs on two separate bands and they have the opposite sign each other. Therefore, we expect a similar mechanism as in the d-wave case to work with the sign-changing ±s-wave superconductors. However, there are important differences: (1) the cancellation of the anomalous selfenergy would not be perfect unless the sizes of +s and −s gap and their corresponding DOSs N_h (hole band DOS) and N_e (electron band DOS) are exactly equal; (2) the DOS of the pure ±s-wave SC state is not linearly vanishing as in the d-wave case but a fully gapped one. Considering these difference and similarity, we need quantitative and transparent investigation of the impurity effects on the ±s-wave state to distinguish it from a nodal gap S such as a d-wave state.

[a] e-mail: ykbang@chonnam.ac.kr

This is an Open Access article distributed under the terms of the Creative Commons Attribution-Noncommercial License 3.0, which permits unrestricted use, distribution, and reproduction in any noncommercial medium, provided the original work is properly cited.

Article available at http://www.epj-conferences.org or http://dx.doi.org/10.1051/epjconf/20122300010

2 Formalism

In this paper, we use the T-matrix approximation for the study of impurity scattering. The basic assumption of the T-matrix approximation is that the total impurity density n_{imp} is very small. Then the interference among the different impurities can be ignored and the each impurity behaves as an independent scatterer. As a result, the multiple scattering process from the single impurity can be easily summed and the total impurity effect is obtained by simply multiplying the single impurity result by n_{imp}. For more detailed discussion of the T-matrix formalism, we refer to the Ref.[8, 9]. In this paper, we consider only the non-magnetic and local impurities. The single impurity Hamiltonian is given by

$$H_{imp} = \sum_{k,k'} U_0 c^{\dagger}_{k,\sigma} c_{k,\sigma} \tag{1}$$

where U_0 is the strength of the impurity potential, and $c^{\dagger}_{k,\sigma}$ and $c_{k,\sigma}$ are usual creation and annihilation operators of electrons. Summing the infinite series of the multiple scattering process from a single impurity potential, the full Green function of the electron is written as

$$\hat{g}(\omega_n, k) = \hat{g}_0(\omega_n, k) + \hat{g}_0(\omega_n, k)\hat{T}(\omega_n)\hat{g}_0(\omega_n, k) \tag{2}$$

where the "$\hat{..}$" symbol means the matrix form in the SC state but it becomes a scalar quantity in the normal metallic state, and $\omega_n = \pi T(2n+1)$ is the Matsubara frequency. The non-interaction Green function in the SC state is given as

$$\hat{g}_0(\omega_n, k) = [i\omega_n\tau_1 + \epsilon(k)\tau_3 + \Delta(k)\tau_1]^{-1}. \tag{3}$$

where τ_i is the Pauli matrix in the particle-hole space and we drop the spin indices because we consider only the spin singlet superconductors in this paper. For the local (or delta function) potential, the T-matrix becomes k-independent and given as

$$\hat{T}(\omega) = \hat{U}_0 \cdot [1 - \hat{U}_0 \sum_k \hat{g}_0(\omega, k)]^{-1}. \tag{4}$$

with the matrix form of the impurity potential $\hat{U}_0 = U_0\tau_3$. As can be seen in the above equation, in the T-matrix formalism, $\hat{g}_0(\omega, k)$ always comes with the total momentum summation as $\sum_k \hat{g}_0(\omega, k)$. Therefore it is convenient to define the following momentum integrated Green functions for each Pauli component

$$G^0_0(\omega) = \frac{1}{\pi N_0}\sum_k g^0_0(\omega, k) = \left\langle \frac{\omega_n}{\sqrt{\omega_n^2 + \Delta^2(k)}} \right\rangle, \tag{5}$$

$$G^1_0(\omega) = \frac{1}{\pi N_0}\sum_k g^1_0(\omega, k) = \left\langle \frac{\Delta(k)}{\sqrt{\omega_n^2 + \Delta^2(k)}} \right\rangle, \tag{6}$$

$$G^3_0(\omega) = \frac{1}{\pi N_0}\sum_k g^3_0(\omega, k) = 0. \tag{7}$$

$$\tag{8}$$

Above we integrated over the momentum k only for the component perpendicular to the Fermi surface (FS) and the component parallel to the FS remained. The symbol "$\langle ... \rangle$" means the FS angle average. From this, it is clear that the second equation for $G^1_0(\omega)$ should vanish for the d-wave S. The last equation for $G^3_0(\omega)$ is identically zero with the particle-hole symmetry assumption which is practically satisfied for all metallic system.

Now using Eq.(4), we can calculate the T-matrices and the previous discussion of the particle-hole symmetry allow us to take $T^3 = 0$ in general and we need to calculate $T^{0,1}$ components only. Instead of using the impurity potential strength U_0, it is more convenient to introduce the phase shift parameter c defined as $\pi N_0 U_0 = c^{-1} = \tan\delta_0$ related to the s-wave phase shift δ_0; with c=0 in the unitary limit and $c > 1$ in the Born limit scattering. To this end, $T^{0,1}$ are solved as

$$T^i(\omega_n) = \frac{G^i(\omega_n)}{D} \quad (i = 0, 1), \tag{9}$$

$$D = c^2 + [G^0]^2 + [G^1]^2, \tag{10}$$

$$G^0(\omega_n) = \left\langle \frac{\tilde{\omega}_n}{\sqrt{\tilde{\omega}_n^2 + \tilde{\Delta}^2(k)}} \right\rangle, \tag{11}$$

$$G^1(\omega_n) = \left\langle \frac{\tilde{\Delta}}{\sqrt{\tilde{\omega}_n^2 + \tilde{\Delta}^2(k)}}, \right\rangle \tag{12}$$

Finally, the impurity induced selfenergy correction is given as $\Sigma^i(\omega_n) = \Gamma T^i(\omega_n)$ with the impurity concentration parameter $\Gamma = n_{imp}/(\pi N_0)$ and in turn these selfenergies renormalize the Green functions as $\tilde{\omega}_n = \omega_n + \Sigma^0$ and $\tilde{\Delta} = \Delta + \Sigma^1$, respectively.

2.1 d-wave state

The d-wave state has the property that the FS angle average of the OP, $< \Delta(k) >$ becomes zero. Therefore, the T^1 component is identically zero and the T^0 component is given by

$$T^0(\omega_n) = \frac{G^0(\omega_n)}{c^2 + [G^0]^2}. \tag{13}$$

Now the physical quantities should be calculated by the analytic continuation of $i\omega_n \to \omega + i\delta$. This can be done by two methods: (1) direct numerical substitution of $i\omega_n \to \omega + i\delta$; (2) Pade-approximant method [13]. Either method works well. The retarded form of selfenergy is $\Sigma^0(\omega) = \Gamma T^0(\omega)$ and the various physical quantities are calculated with the renormalized retarded Green function given as

$$\hat{g}(\omega, k) = [\tilde{\omega}\tau_1 - \epsilon(k)\tau_3 - \Delta(k)\tau_1]^{-1}. \tag{14}$$

with $\tilde{\omega} = \omega + \Sigma^0(\omega)$.

For example, assuming the FS angle dependent d-wave OP $\Delta(\phi)$, the DOS is given as

$$N(\omega) = \left\langle Re\frac{\tilde{\omega}}{\sqrt{\tilde{\omega}^2 - \Delta^2(\phi)}} \right\rangle_{\phi}. \tag{15}$$

And we can calculate the nuclear spin-lattice relaxation rate $1/T_1$ following the standard formula

$$\frac{1}{T_1 T} \sim -\int_0^{\infty} d\omega \frac{\partial f_{FD}(\omega)}{\partial \omega} \left[\left\langle Re\frac{\tilde{\omega}}{\sqrt{\tilde{\omega}^2 - \Delta^2(\phi)}} \right\rangle_{\phi}^2 + \left\langle Re\frac{\Delta(\phi)}{\sqrt{\tilde{\omega}^2 - \Delta^2(\phi)}} \right\rangle_{\phi}^2 \right], \tag{16}$$

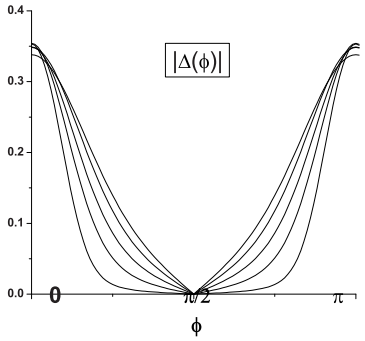

Fig. 1. (Color online) The d-wave OPs $|\Delta(\phi)|$ with different nodal slopes. From Ref.[14].

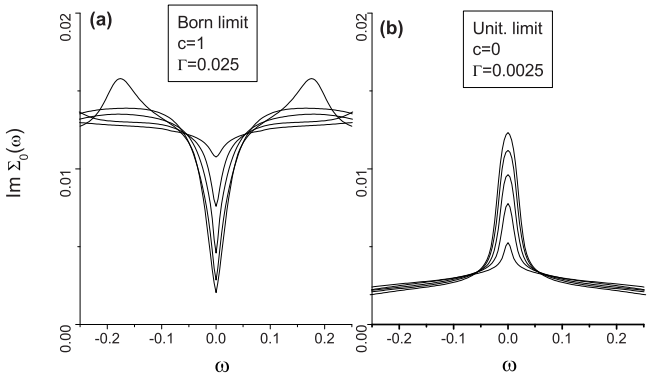

Fig. 2. (Color online) (a) The imaginary part of self-energy $Im\Sigma_0(\omega)$ for different d-wave OP $|\Delta(\phi)|$ shown in Fig.1 with Born limit scatterer ($c = 1$ and $\Gamma = 0.025$). The flatter the nodal region of $|\Delta(\phi)|$ is, the value of $\gamma = Im\Sigma_0(\omega = 0)$ increases; (b) the same as (a) with the unitary scatterer ($c = 0$ and $\Gamma = 0.0025$). The flatter the nodal region of $|\Delta(\phi)|$ is, the value of $\gamma = Im\Sigma_0(\omega = 0)$ decreases. From Ref.[14].

and the superconducting spin susceptibility χ_S

$$\chi_S \sim -\int_0^\infty d\omega \frac{\partial f_{FD}(\omega)}{\partial \omega} \left\langle Re \frac{\tilde{\omega}}{\sqrt{\tilde{\omega}^2 - \Delta^2(\phi)}} \right\rangle_\phi , \quad (17)$$

where $f_{FD}(\omega)$ is the Fermi-Dirac function and $\langle ... \rangle_\phi$ means the angular average over the FS. The first term in the bracket of Eq. (16) is $N^2(\omega)$. The second term vanishes in our calculations because of the symmetry of the OP. To calculate $1/T_1T$ using Eq. (16), or χ_S using Eq. (17), we need the full temperature dependent gap function $\Delta(\phi, T)$ and T_c and we use the phenomenological formula $\Delta(\phi, T) = \Delta(\phi, T = 0)\ \Xi(T)$ with $\Xi(T) = \tanh(\beta\sqrt{T_c/T - 1})$ with parameters β and Δ_0/T_c. In our numerical calculations we chose $\beta = 1.74$, and the final results are not sensitive to this parameter, while the ratio Δ_0/k_BT_c is an important parameter to simulate strong-coupling effects; $\Delta_0/k_BT_c = 2.14$ for the standard weak-coupling d-wave SC and the strong-coupling effects will increase this ratio. The temperature dependence of $\Sigma^0(\omega, T) \equiv \Gamma T^0(\omega, T)$ is similarly extrapolated: $T^0(\omega, T) = T^0(\omega, T = 0)\ \Xi(T) + T_{normal}(1 - \Xi(T))$, where $T_{normal} = \Gamma/(c^2 + 1)$ is the normal state T^0.

Now we show the numerical calculations for the impurity effects on the d-wave SC state. Figure 1 shows the d-wave OP $|\Delta(\phi)|$ with different slopes around the nodal point.[14] The one with the slope near 45 degree is the standard harmonic d-wave OP and the ones with a very flat slope can be realized in the cuprate or heavy fermion d-wave Ss with a critical AFM correlation ($\xi_{AFM} \gg 1$). In Fig.2 we shows the imaginary part of self-energy $Im\Sigma_0(\omega)$ for different d-wave OP $\Delta(\phi)$ shown in Fig.1. Fig.2(a) shows the Born limit impurity case with $\Gamma = 0.025$. We see that the flatter the nodal region of $|\Delta(\phi)|$ is, the value of $\gamma = Im\Sigma_0(\omega = 0)$ increases. Fig.2(b) shows the unitary limit impurity case with $\Gamma = 0.0025$. We see the opposite trend compared to the Born scatter. Namely, the flatter the nodal region of $|\Delta(\phi)|$ is, the value of $\gamma = Im\Sigma_0(\omega = 0)$ decreases.

In Fig.3, we show the normalized DOS $N(\omega)/N_0$ calculated with the results of selfenergy in Fig.2. While the impurity induced selfenergy in Fig.2 showed an opposite behavior for the Born and unitary scatters, $N(\omega = 0)/N_0$ displays the same trend with respect to the shape of the OP $|\Delta(\phi)|$. Namely, for both the Born and unitary scatters, the flatter the nodal region of $|\Delta(\phi)|$ is, the value of

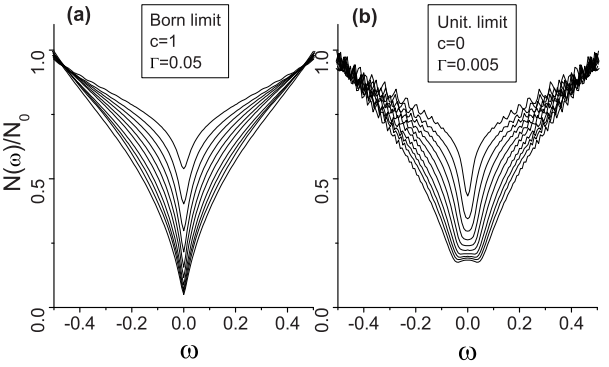

Fig. 3. (Color online) (a) The normalized DOS $N(\omega)/N_0$ for different d-wave OP $|\Delta(\phi)|$ shown in Fig.1 with Born limit scatterer ($c = 1$ and $\Gamma = 0.025$). The flatter the nodal region of $|\Delta(\phi)|$ is, the value of $N(\omega = 0)/N_0$ increases.(b) the same as (a) with the unitary scatterer ($c = 0$ and $\Gamma = 0.0025$). The flatter the nodal region of $|\Delta(\phi)|$ is, the value of $N(\omega)/N_0$ increases. From Ref.[14].

$N(\omega)/N_0$ increases. However, for the standard harmonic d-wave (with 45 degree of slope) case, the shape DOS near zero frequency shows the different behaviors for the Born and unitary impurities, respectively; the DOS remains V-shape with the Born scatterer but the DOS become flat near zero frequency with the unitary scatterer.

Figure 4 shows the calculations of Knight shift $\chi_S(T)$ of a standard harmonic d-wave S normalized by its normal state value χ_N with the gap values $2\Delta_0 = 5\, k_BT_c$ (lines) and $8\, k_BT_c$ (symbols), for pure case and unitary impurity scattering of $\Gamma/\Delta_0 = 0.032$, respectively. As seen in the DOS of the harmonic d-wave case with the unitary scatterer in Fig.3(b), the unitary impurity scattering also makes the low temperature part of $\chi_S(T)$ flat.

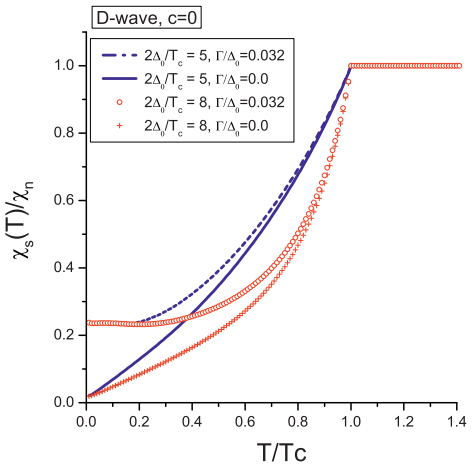

Fig. 4. (Color online) The calculated spin susceptibility χ_S of a standard harmonic d-wave S normalized by its normal state value χ_N for gap values $2\Delta_0 = 5\,k_BT_c$ (lines) and $8\,k_BT_c$ (symbols), and impurity scattering rates $\Gamma/\Delta_0 = 0$ and 0.032, respectively. From Ref.[15].

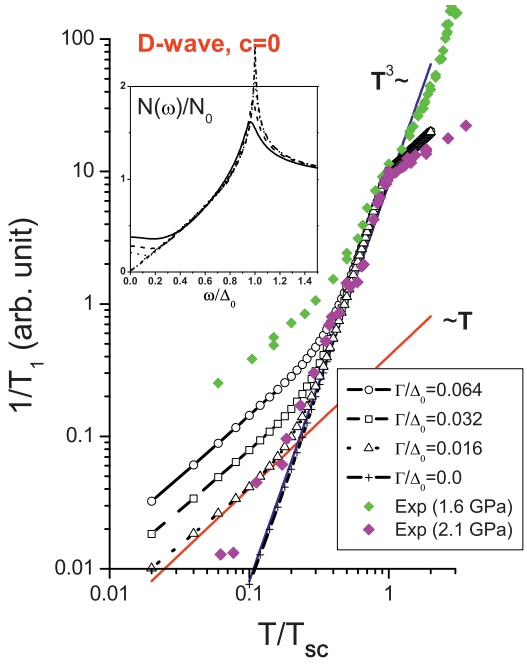

Fig. 5. (Color online) The normalized $1/T_1$ for a standard harmonic d-wave gap for unitary scatterer ($c = 0$) with impurity scattering rates $\Gamma/\Delta_0 = 0.064, 0.032, 0.016, 0.0$. The green diamonds are the normalized 1.6 GPa experimental data and the magenta diamonds are for 2.1 GPa data of $CeRhIn_5$ [16,17]. Solid lines for T^3 and T are guides for the eyes. Inset: The corresponding normalized DOS $N(\omega)/N_0$, in decreasing order of $N(\omega = 0)$, with $\Gamma/\Delta_0 = 0.064, 0.032, 0.016, 0.0$. From Ref.[18].

Figure 5 shows the calculations of the normalized NMR spin lattice relaxation rate $1/T_1$ for a standard harmonic d-wave gap for unitary scatterer ($c = 0$) with different impurity scattering rates $\Gamma/\Delta_0 = 0.0, 0.016, 0.032, 0.064$, respectively. The pure d-wave case shows the well known T^3 behavior and increasing the impurity concentration n_{imp} (equally increasing Γ values), the zero energy impurity resonance density increases as shown in the inset of Fig.5. As a result, $1/T_1$ displays the T-linear part at low temperatures for the increasingly wider region with increasing Γ.

2.2 ±s-wave state

In the minimal two band model of the ±s-wave state [6], there exist two separate bands, hole band and electron band with the DOSs N_h and N_e, respectively. Each band develops an isotropic s-wave OPs, Δ_h and Δ_e, with the opposite sign each other. The impurity effects on this model also can be calculated by the T-matrix formalism but it need to be generalized for the two bands [12] as follows.

$$\mathcal{T}_a^i(\omega_n) = \frac{G_a^i(\omega_n)}{D} \quad (i = 0, 1;\ \ a = h, e), \tag{18}$$

$$D = c^2 + [G_h^0 + G_e^0]^2 + [G_h^1 + G_e^1]^2, \tag{19}$$

$$G_a^0(\omega_n) = \frac{N_a}{N_{tot}} \left\langle \frac{\tilde{\omega}_n}{\sqrt{\tilde{\omega}_n^2 + \tilde{\Delta}_a^2(k)}} \right\rangle, \tag{20}$$

$$G_a^1(\omega_n) = \frac{N_a}{N_{tot}} \left\langle \frac{\tilde{\Delta}_a}{\sqrt{\tilde{\omega}_n^2 + \tilde{\Delta}_a^2(k)}}, \right\rangle \tag{21}$$

where $\tilde{\omega}_n = \omega_n + \Sigma_h^0(\omega_n) + \Sigma_e^0(\omega_n)$ and $\tilde{\Delta}_{h,e} = \Delta_{h,e} + \Sigma_h^1(\omega_n) + \Sigma_e^1(\omega_n)$, and the impurity induced selfenergies are calculated with T-matrices as $\Sigma_{h,e}^{0,1}(\omega_n) = \Gamma \cdot T_{h,e}^{0,1}(\omega_n)$; $\Gamma = n_{imp}/\pi N_{tot}$ where n_{imp} is the impurity concentration and $N_{tot} = N_h + N_e$ is the total DOS.

Note Eq.(19), which is the denominator of T-matrices. The last term of it, $[G_h^1 + G_e^1]$, would exactly vanish for a d-wave and that is the technical reason for the formation of the resonance bound state at zero energy when $c = 0$, the unitary limit scattering. For the ±s-wave case, G_h^1 and G_e^1 have opposite signs, therefore a large cancellation in $[G_h^1 + G_e^1]$ occurs but never be perfect unless $\Delta_e = -\Delta_h$ and $N_h = N_e$. With an incomplete cancellation, the finite remnant acts as weakening the scattering strength c (it means increasing the effective value of c). For the middle term $[G_h^0 + G_e^0]$, G_h^0 and G_e^0 are always the same sign, so that the normal scattering process is additive with number of bands.

With the typical band structure of the Fe-based pnictides[19], $N_h(0)$ and $N_e(0)$ are not equal. Then we showed that the inverse relation between two ratios $N_h(0)/N_e(0)$ and $|\Delta_h|/|\Delta_e|$.[6] This inverse relation between the gap sizes and the DOS sizes – i.e, $|\Delta_h| < |\Delta_e|$ for $N_h(0) > N_e(0)$ and vice versa – is a generic property of the interband pairing model [6]. In this review, we showed the numerical results with the choice of $|\Delta_e|/|\Delta_h| \approx 2.5$ and $N_h(0)/N_e(0) \approx 2.6$.

The NMR nuclear spin-lattice relaxation rate $1/T_1$ of the ±s-wave state is calculated by

$$\frac{1}{T_1} \propto -T \int_0^\infty d\omega \frac{\partial f_{FD}(\omega)}{\partial \omega} \left\{ \sum_{a=h,e} N_a^2(0) \left[\left\langle Re \frac{\tilde{\omega}}{\sqrt{\tilde{\omega}^2 - \tilde{\Delta}_a^2(k)}} \right\rangle_k^2 + \left\langle Re \frac{\tilde{\Delta}_a(k)}{\sqrt{\tilde{\omega}^2 - \tilde{\Delta}_a^2(k)}} \right\rangle_k^2 \right] + 2N_h(0)N_e(0) \left[\right. \right.$$

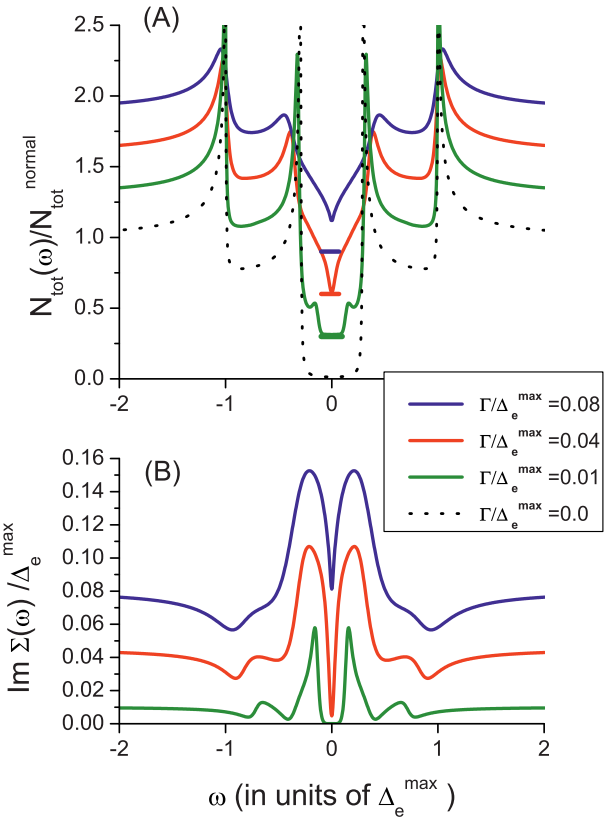

Fig. 6. (Color online) (a) Normalized DOS $N_{tot}(\omega)$ of the ±s-wave S for different impurity concentrations, $\Gamma/\Delta_e = 0.0, 0.01, 0.04, 0.08$. Thin dotted line is of the pure state for comparison and other lines are offset for clarity (the zero baselines of the offset are marked by the narrow horizontal bars of the corresponding colors). (b) Impurity induced selfenergies $Im\Sigma^0_{tot}(\omega) = Im\Sigma^0_h + Im\Sigma^0_e$ with the same parameters as in (a). These curves are not offset. From Ref.[12].

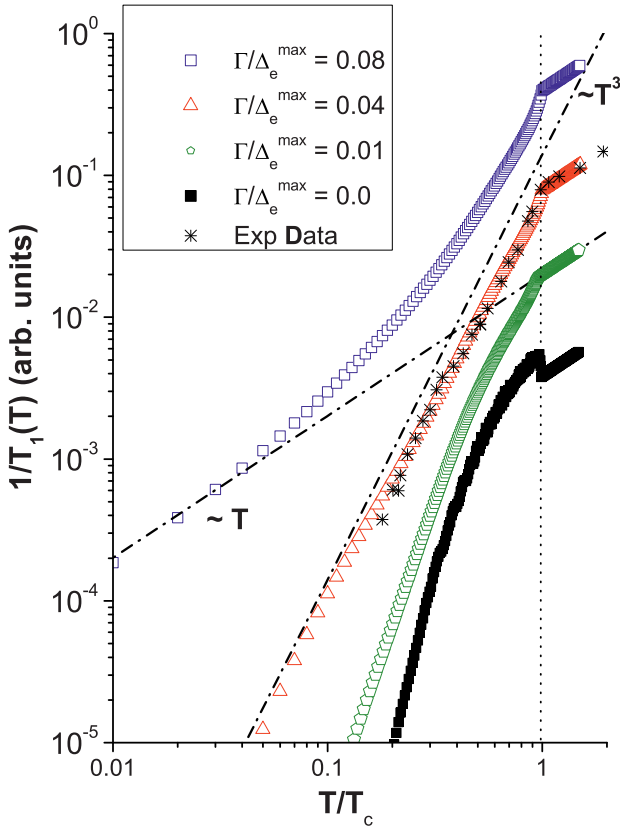

Fig. 7. (Color online) Calculated $1/T_1(T)$ of the ±s-wave S for different impurity concentrations, $\Gamma/\Delta_e = 0.0, 0.01, 0.04, 0.08$ and with $2\Delta_h/T_c$=3.0. Experimental data is from Ref.[22]. The curves are offset for clarity. From Ref.[12].

$$\left\langle Re\frac{\tilde{\omega}}{\sqrt{\tilde{\omega}^2-\tilde{\Delta}_h^2(k)}}\right\rangle_k \left\langle Re\frac{\tilde{\omega}}{\sqrt{\tilde{\omega}^2-\tilde{\Delta}_e^2(k')}}\right\rangle_{k'} + \left\langle Re\frac{\tilde{\Delta}_h(k)}{\sqrt{\tilde{\omega}^2-\tilde{\Delta}_h^2(k)}}\right\rangle_k \left\langle Re\frac{\tilde{\Delta}_e(k')}{\sqrt{\tilde{\omega}^2-\tilde{\Delta}_e^2(k')}}\right\rangle_{k'} \Bigg]\Bigg\}. \quad (22)$$

The above formula of $1/T_1$ contains three scattering channels: two intraband scattering channels from the hole band and electron band, respectively, and one interband scattering channel between the hole and electron bands. The unique feature of the ±s-wave state is the interband scattering channel. Having the opposite signs for Δ_h and Δ_e, this term (the last term in Eq.(22)) substantially cuts out the relaxation rate below T_c, reducing the so-called Hebel-Schlichter peak. However, we emphasized that this interband term is not sufficient enough to completely wash out the Hebel-Schlichter peak, in particular, when the other two intraband scattering processes are correctly included [6]. Our results shows that the impurity scattering is necessary to completely kill the Hebel-Schlichter peak. For the temperature dependence of the gaps $\Delta_{h,e}(k,T)$, we use a phenomenological formula, $\Delta_{h,e}(k,T) = \Delta_{h,e}(k)\tanh(\beta\sqrt{T_c/T-1})$, as in the d-wave case.

Fig.6 (a) shows the total DOS of two bands with different impurity concentrations $\Gamma/\Delta_e = 0.0, 0.01, 0.04, 0.08$ of the unitary scatterer (c=0), and Fig.6(b) shows the corresponding impurity induced selfenergy $Im\Sigma^0_{tot}(\omega) = Im\Sigma^0_h + Im\Sigma^0_e$. Fig.6 (a) shows how the fully opened gap of the pure state is filled with impurity states; the pattern of filling is very unusual and the $\Gamma/\Delta_e = 0.04$ case displays a perfect V-shape DOS down to zero energy mimicking the pure d-wave SC gap. The origin of this behavior is easily seen in Fig.6(b); the impurity bound state is never formed at zero energy but away from it (even in the unitary limit) because of the incomplete cancellation of $[G^1_h + G^1_e]$, so *the full gap around* $\omega = 0$ *is protected* until this off-centered impurity band spills over to the zero energy with increasing the impurity concentration. When it touches the zero energy, the superconductor behaves gapless as in a pure d-wave superconductor, and this happens with the critical impurity concentration Γ_{crit} ($= 0.04\Delta_e$ in our specific model calculations). Increasing the impurity concentration beyond Γ_{crit}, the DOS still keeps the V-shape but now $N_{tot}(\omega = 0)$ obtains a finite value (see the blue curve of $\Gamma = 0.08\Delta_e$ case in Fig.6(a)).

This manner of evolution of the DOS with the impurity concentration results in the following consequences: (1) Beyond the critical impurity concentrations, direct measurements of the DOS at low temperature such as photoemission and tunnelling spectroscopy would see a V-shape DOS, but at the same time ARPES would be measuring an

isotropic gap [20,21]; (2) Temperature dependence measurement such as $1/T_1(T)$ would see three different types of behavior. First, when $\Gamma = \Gamma_{crit}$ ($\Gamma = 0.04\Delta_e$ case in Fig.6(a)), the system sees the linear in ω DOS for whole temperature region of $0 < T < T_c$. Second, when $\Gamma > \Gamma_{crit}$ ($\Gamma = 0.08\Delta_e$ case in Fig.6(a)), the linear in ω DOS will prevail in the high temperature region, but at low temperatures the finite DOS of $N_{tot}(\omega = 0)$ makes the system a gapless superconductor. Finally, when $\Gamma < \Gamma_{crit}$ ($\Gamma = 0.01\Delta_e$ case in Fig.6(a)), the system always behaves as a fully opened gap superconductor although the gap is weakened by impurities. This variation of DOS with the impurity concentration will be reflected in the behavior of $1/T_1(T)$ as shown in Fig.7.

Figure 7 shows the calculations of $1/T_1(T)$ with the variation of the impurity concentration using the same parameters as in Fig.6. It is clear that the puzzling T^3 behavior of $1/T_1$ can be understood with the ±s-wave; it has the same origin as in the d-wave gap, i.e., the linearly rising DOS. With $\Gamma = \Gamma_{crit} = 0.04\Delta_e$, the T^3 behavior extends to the lowest possible temperatures as expected. With $\Gamma > \Gamma_{crit}$, the T^3 behavior occurs only at high temperatures and at lower temperatures the system probes the finite DOS of $N_{tot}(\omega = 0)$, hence displaying the T-linear behavior of $1/T_1$. With $\Gamma < \Gamma_{crit}$, the system should display a full gap behavior below T_c, but somewhat weakened by impurities. As a consequence, $1/T_1$ shows, in this case, a much weakened exponential drop for the extended temperature region below T_c. This wide range of variation occurs with the impurity concentration $0 < \Gamma/\Delta_e < 0.08$ and the reduction of T_c due to impurities is less than 10%; $\delta T_c/T_c^0$ is proportional to $(\Gamma/\Delta_e)/[c^2 + 1]$.

3 Conclusion

In this review, I provided a pedagogical introduction of the T-matrix formalism to study the impurity effects on the SC state. We then studied the impurity scattering effects on two typical unconventional Ss: the d-wave and ±s-wave state. In both cases, the strong limit impurity scatter (unitary scatterer) forms an impurity resonance inside the SC gap and it significantly changes the low energy properties of both SC states. However, there is also important difference between two cases; the d-wave state has the zero energy resonance but the ±s-wave state has an off-centered resonance, respectively. We showed the numerical calculations of the impurity induced selfenergy, the modified DOS, Knight shift, and NMR $1/T_1$ relaxation rates for both SC states for the comparative studies. I hope that the readers obtain a good guideline to read the experimental data to distinguish the different unconventional superconductors.

References

1. Y. Kamihara et al., J. Am. Chem. Soc., **128**, 10012 (2006); Y. Kamihara et al., J. Am. Chem. Soc., **130**, 3296 (2008).
2. G. F. Chen et al., Phys. Rev. Lett. **100**, 247002 (2008); G. F. Chen et al., Nature **453**, 761 (2008).
3. I.I. Mazin, D.J. Singh, M.D. Johannes, M.H. Du, Phys. Rev. Lett. **101**, 057003 (2008).
4. K. Kuroki et al., Phys. Rev. Lett. **101**, 087004 (2008).
5. M.M. Korshunov and I. Eremin, Phys. Rev. B **78**, 140509(R) (2008).
6. Y. Bang and H.-Y. Choi, Phys. Rev. B, **78**, 134523 (2008).
7. F. Wang, H. Zhai, Y. Ran, A. Vishwanath, Dung-Hai Lee, Phys. Rev. Lett. **102**, 047005 (2009).
8. A. V. Balatsky, I. Vekhter, and J.-X. Zhu, Rev. Mod. Phys. **78**, 373 (2006) and see more references therein.
9. P. J. Hirschfeld, P. Wolfle, and D. Einzel, Phys. Rev. B **37**, 83 (1988); A. V. Balatsky, I. Vekhter, and J.-X. Zhu, Rev. Mod. Phys. **78**, 373 (2006) and see more references therein.
10. L. S. Borkowski and P. J. Hirschfeld Phys. Rev. B **49**, 15404 (1994).
11. N. Curro, T. Caldwell, E.D.Bauer, L.A. Morales, M.J. Graf, Yunkyu Bang, A.V. Balatsky, J.D. Thompson, J.L.Sarrao, Nature **434**, 622 (2005).
12. Y. Bang, H.-Y Choi, H. K. Won, Phys. Rev. B **79**, 054529 (2009).
13. H.J Vidberg and J.W. Serene, J. of Low Temp. Phys. **29**, 179 (1977).
14. Y. Bang, I. Martin, and A. V. Balatsky Phys. Rev. B **66**, 224501 (2002)
15. Y. Bang, M.J. Graf, N.J. Curro, A.V. Balatsky, Phys. Rev. B **74**, 054514 (2006).
16. S. Kawasaki, T. Mito, G.-q. Zheng, C. Thessiue, Y. Kawasaki, K. Ishida, Y. Kitaoka, T. Muramatsu, T.C. Kobayashi, D. Aoki, S. Araki, Y. Haga, R. Settai, and Y. Onuki, Phys. Rev. B **65**, 020504 (2001); S. Kawasaki, T. Mito, Y. Kawasaki, G.-q. Zheng, Y. Kitaoka, D. Aoki, Y. Haga, Y. Onuki, Phys. Rev. Lett. **91**, 137001 (2003).
17. T. Mito, S. Kawasaki, G.-q. Zheng, Y. Kawasaki, K. Ishida, Y. Kitaoka, D. Aoki, Y. Haga, and Y. Onuki , Phys. Rev. B **63**, 220507 (2001).
18. Y. Bang, M. J. Graf, A. V. Balatsky, and J. D. Thompson, Phys. Rev. B **69**, 014505 (2004)
19. D.J. Singh and M.-H. Du, Phys. Rev. Lett. **100**, 237003 (2008) ; C. Cao, P. J. Hirschfeld, H.P. Cheng, Phys. Rev. B **77**, 220506(R) (2008); E. Manousakis, Jun Ren, E. Kaxiras, Phys. Rev. B **78**, 205112 (2008).
20. L. Shan et al., Europhys. Letters, **83**, 57004 (2008).
21. H. Ding et al., Europhys. Lett. **83**, 47001 (2008); T. Kondo et al., Phys. Rev. Lett. **101**, 147003 (2008).
22. S. Kawasaki et al., Phys. Rev. B **78**, 220506(R) (2008).